Limnol. Oceanogr., 43(6), 1998, 1180–1197

Laboratory measurements of angular distributions of light scattered by phytoplankton and silt

H. Volten, J. F. de Haan, J. W. Hovenier, R. Schreurs, and W. Vassen
Department of Physics and Astronomy, Free University,
De Boelelaan 1081, NL-1081 HV Amsterdam, The Netherlands

A. G. Dekker and H. J. Hoogenboom
Institute for Environmental Studies, Free University,
De Boelelaan 1115, NL-1081 HV Amsterdam, The Netherlands

F. Charlton
Institute for Freshwater Ecology, Ferry House, Far Sawrey,
Ambleside, Cumbria LA22 DEN, England

R. Wouts
Netherlands Institute of Ecology, Centre for Estuarine Coastal Ecology, P.O. Box 140, 4400 AC Yerseke, The Netherlands

Abstract

We present laboratory measurements of scattering properties of 15 different types of coastal and inland water phytoplankton species and two types of estuarine sediments. These properties are the scattering function as well as the angular distribution of a ratio of scattering matrix elements, which in practice equals the degree of linear polarization of the scattered light if the incident light is unpolarized. Laser light with a wavelength of 633 nm was used, and a scattering angle range from 20° to 60° was covered. The results can be used in the context of water-quality studies and to test results of theoretical models. The measured scattering functions are all strongly peaked in forward directions, but not equally so. For the covered angles, they vary significantly as a function of scattering angle. The measured angular distributions of the degree of linear polarization are mostly bell shaped, showing a maximum near 90°, whose magnitude is clearly different for the phytoplankton compared to the silt particles. We find that the morphology and structural features of the particles studied play an important and complex role in their light-scattering behavior. In particular, internal cell structures such as gas vacuoles alter the scattering patterns of the phytoplankton species considerably. The external shape of the cells appears to have a much smaller influence. The experimental results are compared with results of Mie calculations and with the "standard scattering function" of San Diego Harbor water. In most cases, Mie calculations cannot provide an adequate approximation of the measured scattering behavior, which indicates that more sophisticated models are required. Only 3 of the 17 measured scattering functions resemble the San Diego Harbor standard scattering function. One of these pertains to small silt particles, showing that this function is representative for water dominated by these particles.

Diverse particles occur in coastal and inland waters, such as phytoplankton particles (i.e., cyanobacteria and algae), detritus (organic nonliving particles), and mineral particles (Dekker 1993; Mobley 1994). The scattering and absorption properties of these particles are interesting from various points of view, as discussed below.

Theoretical models describing light scattering by small particles have evolved during many decades. It is possible to solve Maxwell's equations for spherical particles (Mie 1908) and for nonspherical particles having simple shapes (cylinders, spheroids, and fluffy particles) with methods such as the T-matrix method and the discrete dipole approximation (e.g., *see* Hovenier [1996] and references therein). It may soon become possible to perform calculations for light scattering by particles with more complicated internal or external structures. However, because it often takes a lot of effort to extend existing computer programs, it is important to know beforehand whether structural features affect the scattering properties in a significant manner. One way to obtain such information is to perform measurements of the scattering properties of various particles. The results of these measurements may guide the development of theoretical models and can be used to test the calculations. In these

Acknowledgments

We thank J. Bouma for extensive technical support, J. M. M. Tesselaar for making the glass basin and cuvette, and S. Kars for providing SEM photographs of the latex spheres. Furthermore, acknowledgments are due to the Centre for Limnology of the Netherlands Institute of Ecology in Nieuwersluis (The Netherlands) for the use of laboratory facilities, and to M. Rijkeboer for her help with supporting measurements. We are indebted to staff of the Culture Collection of Algae and Protozoa IFE, Windermere, Cumbria, England, for providing phytoplankton cultures. This research was supported by grants from the National Remote Sensing Board (BCRS) and the National Institute for Coastal and Marine Management (RIKZ). We are pleased to express our gratitude to Steven G. Ackleson and an anonymous referee for constructive comments on an earlier version of this paper.

cases, it is important to measure not only the angular distribution of the flux, but also that of the polarization of the scattered light for unpolarized incident light.

Models describing radiative transfer in water have been developed and are being improved (e.g., Mobley 1994). Such models can be used to study and interpret the underwater light climate. This light climate is important for the study of ecosystems, particularly with respect to the growth and decay of phytoplankton. Radiative transfer models rely on the assumption that the single scattering properties of the various constituents are known. Therefore, it is important to have available representative scattering properties of these constituents and to determine how they may differ between waters containing different particles. Presently, one standard model for the scattering properties of turbid waters is generally employed, namely, the volume scattering function of turbid ocean water measured in the San Diego Harbor by Petzold (1972). In this paper, we present new measurements that can be used to determine to what extent this standard function is representative for various water types (e.g., turbid and/or eutrophic inland waters).

Semiempirical methods are often used to interpret remote-sensing images taken above water (*see* sect. 7.4 in Kirk 1994) wherein spectral signatures of the reflection properties of water are used to derive concentrations of water constituents, using so-called water-quality algorithms. For example, one seeks to determine concentrations of chlorophyll *a* (Chl *a*) pigments and silt from remote-sensing images. If, for different water types, the scattering properties of the particles differ significantly, one may expect significant bias in the results obtained from such water-quality algorithms. It is therefore important to know the differences in scattering properties that occur for different water constituents (e.g., Dekker et al. 1995).

Relatively few measurements of the angular distribution of light scattered by hydrosol particles have been reported. Some results for natural waters have been published (Spilhaus 1968; Petzold 1972; Whitlock et al. 1981; Sugihara et al. 1982; Kullenberg 1984; Voss and Fry 1984). Some authors have focused on individual hydrosol species (Privoznik et al. 1978; Morel and Bricaud 1986; Quinby-Hunt et al. 1989; Król et al. 1992; Lofftus et al. 1992; Witkowski et al. 1993), whereas others have measured light scattering by individual particles at a limited number of scattering angles by using flow cytometric techniques (Dubelaar et al. 1987; Ackleson and Spinrad 1988; Ackleson et al. 1993). Comparison of results for various species is difficult, because differences may in part be attributed to the use of different instruments. Some authors have found small differences in the shape of the angular scattering function of various (oceanic) water constituents (Petzold 1972; Voss and Fry 1984), whereas others have found considerable differences (Sugihara et al. 1982).

In 1995, we began charting differences in scattering and absorption properties of various constituents of water that are common in Dutch coastal and inland waters. Phytoplankton samples cultivated under controlled conditions at the Institute for Freshwater Ecology (IFE, England) and at the Netherlands Institute of Ecology, Centre for Estuarine Coastal Ecology (NIOO-CEMO, Yerseke, The Netherlands), as well as two differently sized silt samples, were transported to Amsterdam to measure the angular distribution of light scattered by these small particles. The setup was originally designed for measuring the angular distribution of light scattered by aerosol particles, but has been adapted to measure scattering properties of hydrosol particles. The setup used is a revised and improved version of that described by Stammes (1989), Kuik et al. (1991), and Kuik (1992). Hence, it suffices to describe the adaptations made to perform measurements on hydrosol particles. Here, we report results of measurements of the angular distribution of the flux of the light scattered by 15 different types of phytoplankton and two types of sediment. For checking purposes and to facilitate comparisons with theoretical models, we also report measurements of quantities describing polarization properties of the light scattered by the sample. However, because the phytoplankton samples must be in the exponential phase of growth during measurements, we restricted our measurements pertaining to polarization to two additional elements of the Mueller matrix involved. Furthermore, we compare our results with those of Mie calculations and with the standard function of Petzold (1972). Not all measurements obtained during the project are reported here. Other results, such as spectral absorption properties, will be published elsewhere.

The main purpose of this paper is to provide information on the angular scattering properties of a large set of different hydrosol species. Results can be used (1) to guide development of theoretical models and test their results, (2) to assess differences of angular scattering properties that can be used in studying the underwater light climate, and (3) to evaluate the accuracy of water-quality algorithms used for deriving water-quality parameters from remote-sensing images.

Materials and methods

Description of the hydrosols—We provide below an overview of properties that determine the scattering behavior of hydrosols, such as their shape, structural features, size distribution, and complex refractive index. These properties are listed in Table 1 for the different types of hydrosols studied here. Values of these parameters have been obtained either from additional measurements or, if these were not available, from the literature. The values for size distributions and (complex) refractive indices have been used in Mie calculations. Values of the imaginary part of the refractive index and the width of the size distribution, which could not be obtained in other ways, have been derived from fitting the measurements with Mie calculations (*see below*). We will now discuss columns 3–7 of Table 1.

Particle cell shape and structural features—Phytoplankton (algae and cyanobacteria) show a wide variety of shapes. The shapes listed in Table 1 have been taken from photographs and the literature. Employing classifications frequently encountered in flow cytometry and theoretical light-scattering studies, we distinguish between two main classes—spherically celled species and cylindrically celled species. The remaining species belong to neither class (e.g., the box-

Table 1. Overview of the cell shape, structural features, size distribution, complex refractive index, and N_{meas} (number of light-scattering measurements) of the phytoplankton and sediments under investigation.

Name of hydrosol	Group*	Cell shape	Structural features	Size distribution r_{eff} (μm)	Size distribution v_{eff}	$(m = n - in')$ at λ = 633 nm	N_{meas}
Microcystis aeruginosa	cya	sph	No gas vac	5.23†	0.50†	1.04‖ − *i*0.000§	4
Microcystis aeruginosa	cya	sph	Gas vac	6.83†	0.92†	1.04‖ − *i*0.000§	4
Microcystis sp.	cya	sph	Gas vac	1.87‡	0.063‡	1.02¶ − *i*0.001¶	2
Phaeocystis	pry	sph		12.2†	0.43†	1.04‖ − *i*0.005§	3
Volvox aureus	chl	sph	sph col	105‡	0.07‡	1.24¶ − *i*0.12¶	2
Prochlorothrix hollandica	cya (pro)	cyl	fil	1.55‡	0.080‡	1.24¶ − *i*0.006¶	3
Oscillatoria amoena	cya	cyl	fil	2.58‡	0.002‡	1.05¶ − *i*0.004¶	1
Oscillatoria agardhii	cya	cyl	fil, gas vac	1.64§	0.044§	1.05¶ − *i*0.000§	1
Melosira granulata	bac	cyl	fil	3.74‡	0.004‡	1.02¶ − *i*0.002¶	1
Anabaena flos aquae	cya	sph	fil, gas vac	3.09‡	0.012‡	1.03¶ − *i*0.002¶	2
Astrionella formosa	bac	cyl	star-shaped col	4.23‡	0.010‡	1.03¶ − *i*0.003¶	1
Selenastrum capricornutum	chl	sic		1.09‡	0.037‡	1.24¶ − *i*0.020¶	1
Phaeodactylum	bac	box		16.4†	0.23†	1.04‖ − *i*0.000§	3
Emiliania huxleyi	pry	sph	calcite mantel	1.8‖	0.07§	1.04‖ − *i*0.000§	1
Emiliania huxleyi	pry	sph	no calcite mantel	1.8‖	0.002§	1.04‖ − *i*0.042§	1
Westerschelde silt	—	irr		1.95§	0.50§	1.1# − *i*0.000§	2
Westerschelde silt	—	irr		5.93§	0.00§	1.1# − *i*1.05§	2

* cya, cyanobacteria; chl, chlorophyta; bac, bacillariophycae; pro, prochlorophyta; pry, prymnesiophycae; sph, (more or less) spherical; cyl, (more or less) cylindrical; fil, filamentous; col, colony, gas vac, gas vacuoles; sic, sickle shaped; box, box shaped; irr, irregular.
† Determined with a Coulter counter.
‡ Determined with a microscope.
§ From best fit with Mie calculations.
‖ From Bricaud and Morel (1986).
¶ Calculated following the method of Morel and Bricaud (1986).
# From measurements and anomalous diffraction fit.

shaped and the sickle-shaped species). The silt particles have irregular shapes. Apart from the filamentous species, two other species form colonies. *Astrionella formosa* tends to group itself into star-shaped colonies, and *Volvox aureus* forms spherical colonies, the size distribution of which is given in Table 1 (in contrast to the other species in this table, for which the size distributions of the cells are given).

Algae (here, chlorophyta, bacillariophycae, and prymnesiophycae) can have pronounced internal structures (e.g., chloroplasts, mitochondria, and glycogen-storage structures). Some species are surrounded by calcite plates or silicate mantels. Cyanobacteria have less internal structure than do eukaryotic species. In contrast, gas vacuoles are common in many cyanobacteria species. Gas vacuoles are groups of gas vesicles, which are spindle-shaped rigid structures filled with air, with lengths between 300 and 700 nm and diameters between 60 and 110 nm (Donze et al. 1987; Walsby 1994). These dimensions are more or less the same for all organism types. One cell can contain up to a few hundred gas vacuoles.

Two of the phytoplankton species have been modified for investigating the influence of specific structural features on the scattering pattern. We have performed measurements on *Microcystis aeruginosa* with and without gas vacuoles. Likewise, we studied *Emiliania huxleyi* with calcite mantels and with the calcite mantels removed.

Size distribution—Table 1 lists the effective radius, r_{eff}, and the effective variance, v_{eff}, for volume-equivalent spheres (Hansen and Travis 1974). The volume-equivalent effective radii of cells range from ~1 to 16 μm.

Most size distributions were determined with a microscope or a Coulter counter, i.e., an instrument that measures the change in voltage induced when a particle passes between two small electrodes. This change in voltage is assumed to be proportional to the particle volume (e.g., *see* Sheldon and Parsons 1967). For *Oscillatoria agardhii, E. huxleyi,* and the two differently sized Westerschelde silt samples, no such measurements were performed. For these species, we assumed a gamma size distribution (Hansen and Travis 1974) for which either v_{eff} (for *E. huxleyi*) or both r_{eff} and v_{eff} for volume-equivalent spheres were determined by fitting the measurement results to results of Mie calculations. The effective radius of *E. huxleyi* was taken from Bricaud and Morel (1986).

Refractive index—Throughout this paper, all values for the refractive index ($m = n - in'$) are given relative to water and are valid for a wavelength, λ, of ~633 nm in air.

For some samples, we estimated the real and imaginary part of the refractive index by using cell size and cell number data and absorption measurements, following the method of Morel and Bricaud (1986). This method is not rigorous. However, in the absence of more accurate data, the values thus produced provide a reasonable starting point (e.g., for Mie calculations). We relied on literature data for estimates of the real part of the refractive index for the other phytoplankton samples. Unfortunately, few such values of indi-

vidual phytoplankton species relative to water are available (Carder et al. 1972; Morel and Bricaud 1986; Spinrad and Brown 1986; Ackleson and Spinrad 1988; Stramski and Morel 1990; Ackleson et al. 1993). However, because the chemical composition of the phytoplankton is more or less known, the bulk refractive index can be inferred. This has been done, for example, by Aas (1981), who assumed that phytoplankton consists of a mixture of 70 to >80% water and <20–30% other constituents, i.e., mainly organics. In general, we can conclude that, assuming no internal structures, the bulk real part of the refractive index varies from $n = 1.015$ to 1.08. Following Morel and Bricaud (1986), we adopted $n = 1.04$ for the phytoplankton species for which we could not derive an experimental estimate. For the two size distributions of silt particles, we determined a refractive index $n = 1.1$ from measurements combined with fits to anomalous diffraction theory.

An estimate of the imaginary part of the refractive index (of samples for which we could not derive an estimate otherwise) was obtained from fitting results of Mie calculations to measured elements of the scattering matrix. We followed this procedure rather than choosing one central value, because bulk values of the imaginary part of the refractive index differ considerably for distinct species. However, we can estimate the probable range of n'. Morel and Bricaud (1986) derived a typical value of n' of 0.0025 for absorption due to Chl *a* by assuming a typical value of 1.5% for the ratio of the mass of Chl *a* to the dry mass of an algal cell. The presence of other pigments may increase this value. However, in general, the bulk value of n' is small (<0.01 or 0.02). In some cases, it may become negligible, and the cell can be regarded as transparent.

Some concepts from light-scattering theory—We summarize some concepts from light scattering theory used in this paper. The flux and polarization of a beam of light can be represented by a column vector $I = \{I, Q, U, V\}$, or Stokes vector (*see* sect. 5.12 in Van de Hulst 1957). The Stokes parameter I is proportional to the total flux of the beam. The Stokes parameters Q and U represent differences between two components of the flux for which the electric field vectors oscillate in orthogonal directions. The Stokes parameter V is the difference between two oppositely circularly polarized components of the flux. A plane through the direction of propagation of the beam is chosen as a plane of reference for the Stokes parameters.

If light is scattered by an ensemble of randomly oriented particles and time reciprocity applies, the Stokes vectors of the incident beam and the scattered beam are, for each scattering angle θ, related by a 4×4 scattering matrix as follows (*see* sect. 5.22 in Van de Hulst 1957):

$$\begin{pmatrix} I_s \\ Q_s \\ U_s \\ V_s \end{pmatrix} = \frac{\lambda^2}{4\pi^2 r^2} \begin{pmatrix} F_{11} & F_{12} & F_{13} & F_{14} \\ F_{12} & F_{22} & F_{23} & F_{24} \\ -F_{13} & -F_{23} & F_{33} & F_{34} \\ F_{14} & F_{24} & -F_{34} & F_{44} \end{pmatrix} \begin{pmatrix} I_i \\ Q_i \\ U_i \\ V_i \end{pmatrix}, \quad (1)$$

where the subscript i refers to the incident beam, the subscript s refers to the scattered beam, λ is the wavelength, and r is the distance from the ensemble to the detector. The matrix with elements F_{ij} is called the scattering matrix. Its elements depend on the scattering angle but not on the azimuthal angle. Here, the plane of reference is the scattering plane. The elements F_{ij} contain information about the size parameter, shape, refractive index, and structure of the scatterers.

In this paper, measurements of two matrix elements are presented, F_{11} and F_{12}. A third element, F_{14}, was measured as well, but was found to be identically zero for all samples within the accuracy of the measurements and will further be omitted from the results. For unpolarized incident light, F_{11} is proportional to the flux of the scattered light and is also called scattering function or phase function. For reasons of convenience and tradition, we often refer F_{12} relative to the total flux and use a minus sign. Thus, we use

$$-F_{12}/F_{11} = \frac{I_\perp - I_\parallel}{I_\perp + I_\parallel} \quad (2)$$

where, for unpolarized incident light, $I_\perp$ represents the flux of the scattered light polarized perpendicular to the plane of reference and $I_\parallel$ represents the flux of the scattered light polarized parallel to the plane of reference. The ratio $-F_{12}/F_{11}$ equals the degree of linear polarization of the scattered light if the incident light is unpolarized and if $F_{13} = F_{14} = 0$. Therefore, note that it seems reasonable to assume that $F_{13} \equiv 0$ for most phytoplankton (e.g., Fry and Voss 1985; Voss 1997 pers. comm.) and that our measurements yielded $F_{14} \equiv 0$. Note further that $|-F_{12}/F_{11}| \leq 1$ (*see* Hovenier et al. 1986).

Because we used a relatively long wavelength (633 nm) in our experiment, the influence of inelastic Raman scattering by pure water and fluorescence by pigments in phytoplankton can be neglected (*see* Mobley 1994).

Experimental setup—The experimental setup used to measure the scattering matrix elements of the samples is depicted in Fig. 1. Except for the basin and hydrosol sample holder (Figs. 1, 2), the setup is similar to that developed by Hunt and Huffman (1973) and is a revised and improved version of that described by Stammes (1989), Kuik et al. (1991), and Kuik (1992). The angles of optical elements are measured counterclockwise when looking in the direction of propagation of the light. Light with a wavelength of 633 nm from a linearly polarized continuous wave HeNe laser (5-mW TEM00, beam diameter 0.8 mm, divergence of 1 mrad) passes through a polarizer (extinction ratio $>1 : 10^{-4}$) oriented at 0° between the scattering plane (horizontal plane) and its optical axis. The linearly polarized light propagates through a low voltage modulator (LM 0202, Gsänger) oriented at −45° between the horizontal plane and its optical axis and is scattered by an ensemble of randomly oriented particles. The scattered light is detected by a photomultiplier tube that moves along a ring 300 mm from the scattering sample. The field of view of the photomultiplier is restricted to ~1.7°, by two pinholes (*see below*). For hydrosol particles, the photomultiplier covers a scattering angle range from 20° (nearly forward scattering) to 160° (nearly backward scattering). The particular configuration of the optical components used in the setup allows us to measure simultaneously the scattering

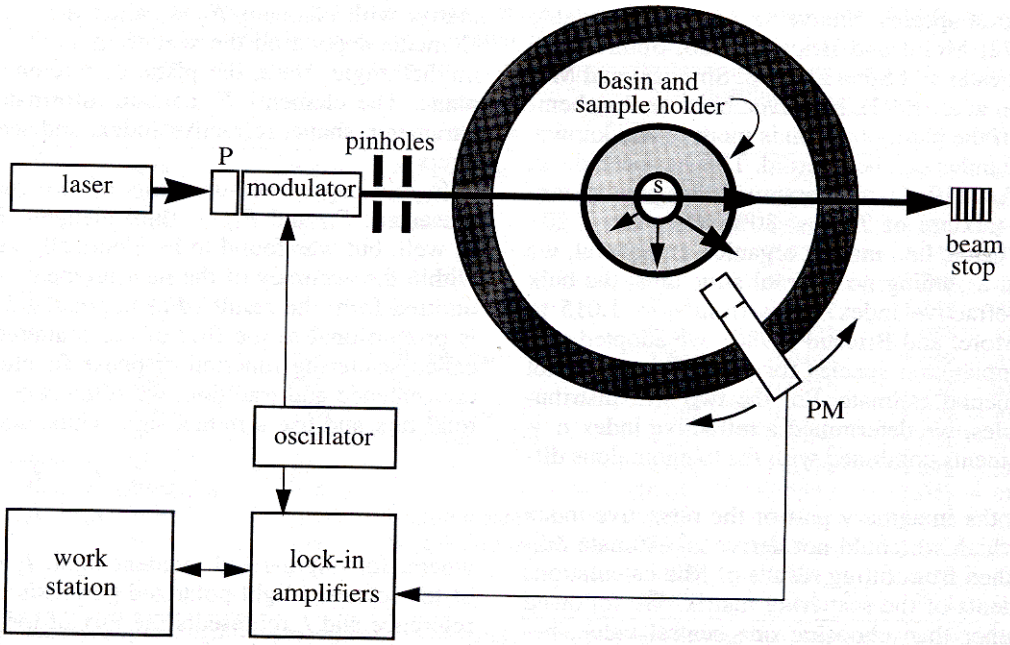

Fig. 1. Schematic picture of the experimental setup. S = sample, P = polarizer, PM = photomultiplier. The laser is a 5-mW HeNe laser (λ = 633 nm). The beam diameter at the scattering center is about 1 mm.

function, $F_{11}(\theta)$, and the matrix elements $F_{12}(\theta)$ and $F_{14}(\theta)$. Other matrix elements can in principle be obtained with different configurations of the optical components (e.g., Kuik et al. 1991, Kuik 1992). The matrix elements are detected either as a direct current signal or as the output of a lock-in amplifier and are then processed on a workstation.

The basin and hydrosol sample holder developed for this research are depicted in Fig. 2. The hydrosol sample is contained in a cylindrically shaped cuvette of Pyrex glass (diameter, 30 mm). The large difference in refractive index between air and the glass cuvette causes strong reflections of the incident light. To reduce the influence of these undesirable reflections, the cuvette was placed in the center of a cylindrical Pyrex glass basin (diameter, 22 cm) filled with glycerine, which has the same refractive index as glass (n = 1.5). Consequently, the strong reflections occur farther away

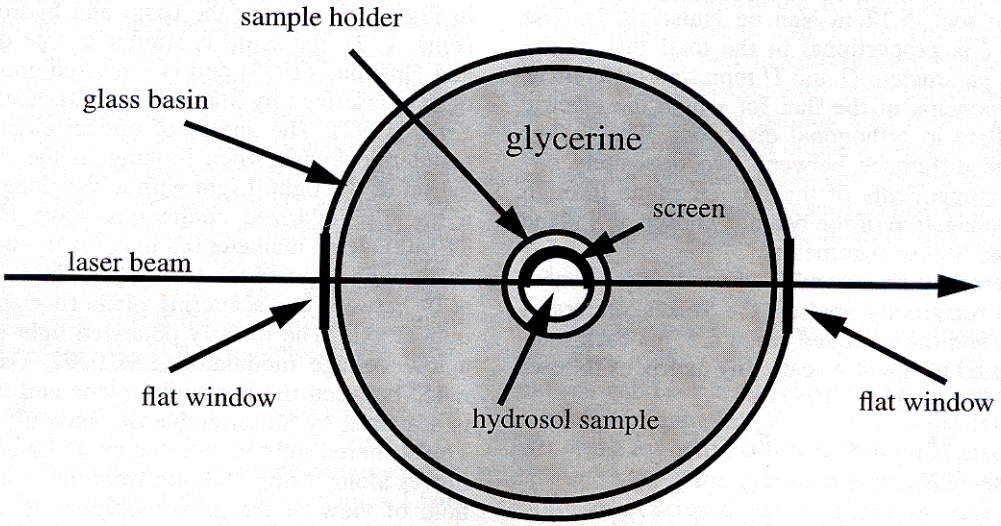

Fig. 2. Enlargement of the basin and hydrosol sample holder in Fig. 1. Both the basin (diameter, 22 cm) and cuvette (inner diameter, 30 mm) are made of Pyrex glass. Glycerine inside the basin is used as a refractive index matching fluid. The basin has 20-mm-wide flat entrance and exit windows. The cuvette inside the basin contains the hydrosol sample and water. It has a screen of blackened copper foil to reduce the influence of reflections.

from the scattering sample. To prevent these reflections from reaching the detector and to avoid spherical aberrations of the beam, the glass basin has flat entrance and exit windows (20 mm wide). In addition, reflections are partly removed from the field of view by placing a semicylindrical screen made of blackened brass foil inside the cuvette.

The Pyrex glass and glycerine do not influence the state of polarization of passing light.

A magnetic stirrer in the cuvette homogenizes the hydrosols continuously. A syringe is used to change the samples in the cuvette, so that the cuvette remains in place and aligned.

Data reduction—Before performing light-scattering measurements, we determined the proper sample concentration to ensure that measurements were in the single scattering regime. After results of the light-scattering measurements were obtained, they were corrected for (1) the changing scattering volume as seen by the rotating detector, (2) background scattering, and (3) reflections at the walls of the sample holder (*see below*).

To avoid multiple scattering, care was taken to use samples with sufficiently low concentrations (e.g., Cross and Latimer 1972; Fry and Voss 1985). By contrast, samples should not be too diluted, since this decreases the signal-to-noise ratio. To determine the optimal sample concentration, the detector was placed at a fixed position at 15°. Subsequently, a series of measurements was made with increasing sample concentration. As long as the scattered flux was proportional to the hydrosol concentration, it was assumed that multiple scattering was negligible. This procedure enables determination of the appropriate sample concentration. We assumed that cells were not damaged by osmotic shock owing to the dilution, since no rapid change in the measured signal just after changing the concentration was observed.

The scattering volume as seen by the detector is determined by the scattering angle, by the geometry of the scattering volume inside the cuvette (length of 30 mm, i.e., diameter of the cuvette, and width of 1 mm, i.e., $2w_0$ of the laser beam), by the distance to the photomultiplier (300 mm), and by the circular pinholes in front of the photomultiplier (one with a diameter of 5 mm directly in front of the tube and one with a diameter of 1 mm 100 mm from it). Taking this geometry into account and assuming that the width of the laser beam can be neglected, correction factors as a function of scattering angle were derived by which the measured flux has to be multiplied to correct for the scattering volume as seen by the detector. This function equals $\sin\theta$ for most of the angle range (*see Fig. 3*), i.e., roughly between 25° and 155° (e.g., *see* sect. 13.2.1 in Bohren and Huffman 1983) and was used to correct the measurements.

Because we explicitly wanted to investigate the light-scattering behavior of the selected hydrosol particles, the amount of light scattered by the background was subtracted from the hydrosol measurement results such that $F_{11} = F_{11}^{\text{meas}} - F_{11}^{\text{backgr}}$ and $F_{12} = F_{12}^{\text{meas}} - F_{12}^{\text{backgr}}$, where F_{11}^{backgr} and F_{12}^{backgr} are results of measurements of the cuvette filled with the same fluid as during the measurements of F_{11}^{meas} and F_{12}^{meas} but without the phytoplankton or silt. We thus ensured that our results are independent of the medium in which particles were

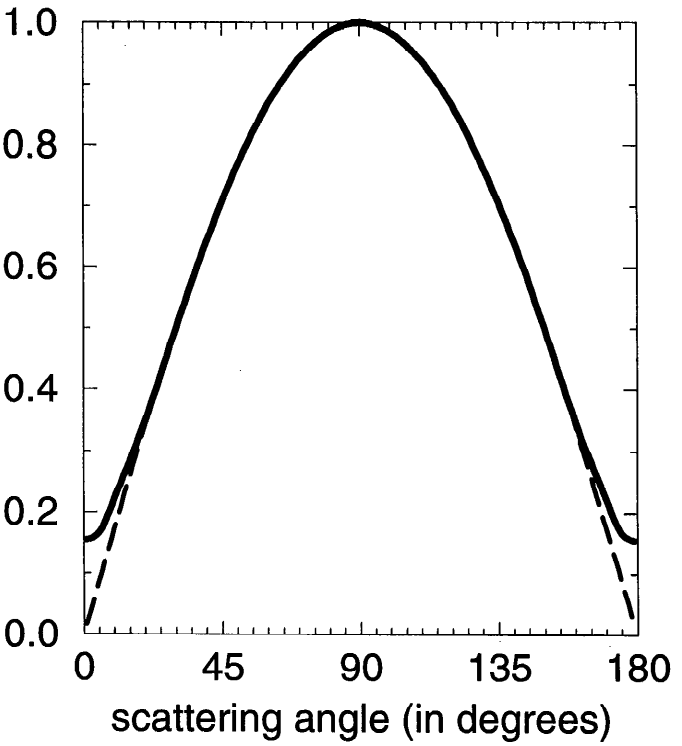

Fig. 3. Correction factors as a function of scattering angle (solid line) by which the measured flux has to be multiplied to correct for the changing scattering volume as seen by the detector. The function equals $\sin\theta$ (dashed line) for most of the angle range.

suspended. This background medium consisted either of demineralized water (demi water) or "Baker-analyzed HPLC" reagent for high-performance liquid chromatography (HPLC water) with various amounts of growing medium, (i.e., water containing nutrients, such as carbohydrates, salts, nitrates, and phosphates, in which the phytoplankton was cultivated). At concentrations <3%, the influence of the growing medium proved to be negligible. Therefore, the growing medium was taken into account for cases where the amount of growing medium with phytoplankton in the sample holder was ≥3% of the total. Measurements of F_{11}^{backgr} and F_{12}^{backgr} of the cuvette filled with demi water, HPLC water, and HPLC water with the appropriate amount of growing medium were performed regularly.

The background correction is significant for measurements where we had to use use low concentrations to avoid multiple scattering. For all measurements, the influence of this correction is most prominent at the smallest and largest scattering angles, where the background signal is strongest (*see* below for an example of F_{11}^{backgr} relative to F_{11}^{meas}; *see* Lofftus et al. 1992).

The hydrosols in the sample scatter the incoming light in all directions. The light scattered toward the screen inside the cuvette is mostly absorbed. However, when direct laser light is reflected by the inner wall of the cuvette or basin, this light follows its trace back, reenters the cuvette, and to some extent is scattered by the hydrosols, etc. The flux of the first-order reflected and then scattered light is propor-

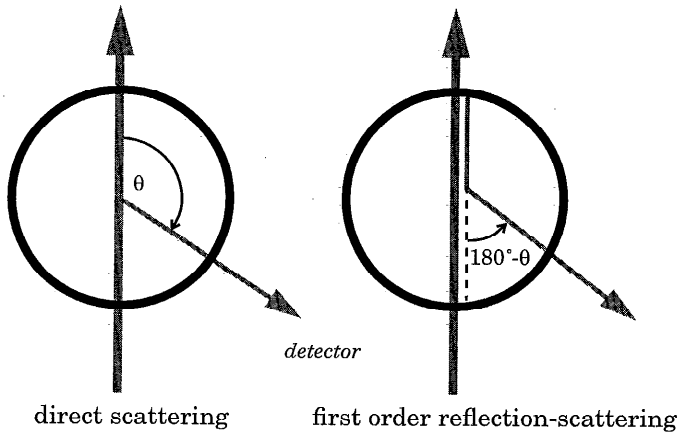

Fig. 4. Comparison of direct scattering by the hydrosols and first-order reflection scattering. The flux of the first-order reflected light is proportional to the scattering function at an angle $180° - \theta$.

tional to $F_{11}(180° - \theta)$ times a reflection coefficient R (*see Fig. 4*). Taking into account multiple reflections, the following expression holds for F_{11}^{uncor}, the measured values, uncorrected for reflections:

$$F_{11}^{\text{uncor}}(\theta) = F_{11}(\theta) + F_{11}(180° - \theta)R + F_{11}(\theta)R^2 + F_{11}(180° - \theta)R^3 + \ldots \quad (3)$$

$$= [F_{11}(\theta) + F_{11}(180° - \theta)R]\frac{1}{1 - R^2} \quad (4)$$

where we used the expression for a geometric series

$$\frac{1}{1 - R^2} = 1 + R^2 + R^4 + R^6 + \ldots \quad (5)$$

and F_{11} represents the true scattering function. The reflection coefficient R has been determined empirically (*see below*). A similar expression follows if we substitute $180° - \theta$ for θ in Eq. 4 and multiply by R, yielding

$$F_{11}^{\text{uncor}}(180° - \theta)R = [F_{11}(180° - \theta) + F_{11}(\theta)R] \times \frac{R}{1 - R^2}. \quad (6)$$

Subtracting Eq. 6 from Eq. 4 yields the following exact expression for the true scattering function (for similar expressions, *see* Sugihara et al. 1982; Schnablegger and Glatter 1993):

$$F_{11}(\theta) = F_{11}^{\text{uncor}}(\theta) - F_{11}^{\text{uncor}}(180° - \theta)R. \quad (7)$$

The same reflection correction has been applied to the $F_{12}(\theta)$ values.

Test measurements on latex spheres—Accuracy of the setup was investigated by comparing results of measurements of latex spheres to results of Mie calculations for spherical particles with a log-normal size distribution having $r_{\text{eff}} = 1.55$ μm, $v_{\text{eff}} = 0.0005$, and refractive index $n - in' = 1.191 - i0.005$, relative to HPLC water (*see Fig. 5*). The values for r_{eff} and n were specified by the manufacturer of the latex spheres (Coulter Electronics); the values for v_{eff} and n' were chosen for providing good agreement between the measurements and Mie calculations. The size distribution of the latex spheres is narrow, causing strong oscillations in the scattering pattern, which makes comparison between theory and measurement more accurate.

To clarify the different steps in the reduction procedure, we show in the left panel of Fig. 5 several intermediate results. We used $R = 0.017$, based on an empirical value for

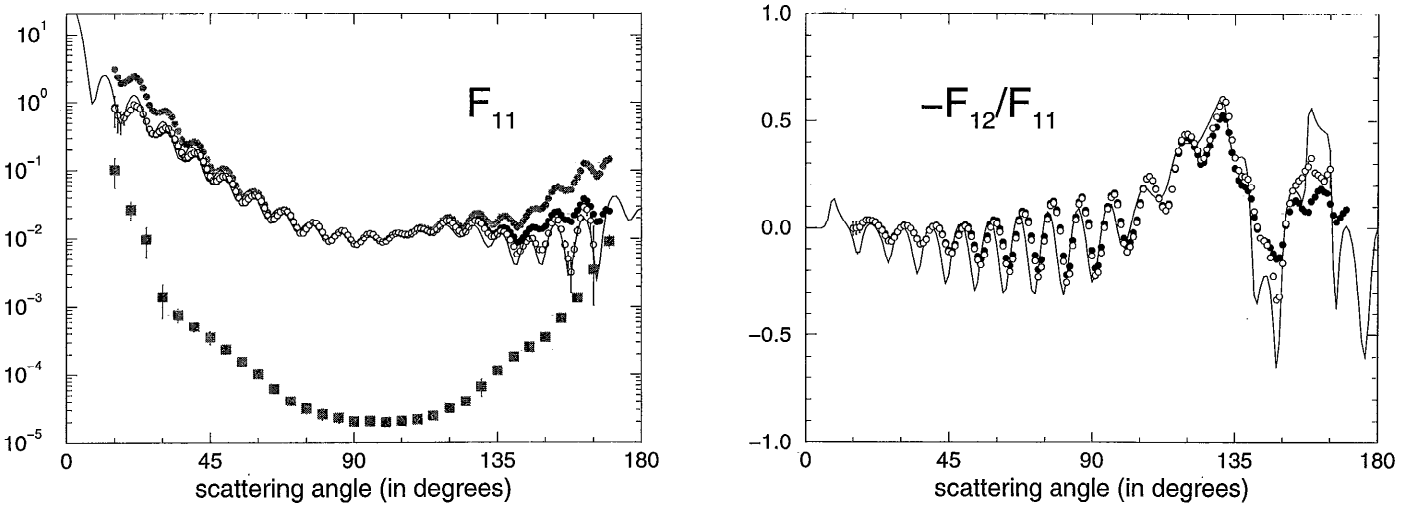

Fig. 5. Intermediate results of the data reduction procedure for the scattering function, F_{11}, for latex spheres are shown in the left panel as a function of scattering angle. The raw uncorrected data are denoted by gray circles. The background measurement that is subtracted from these raw data is shown as gray squares. Subsequent correction for the changing scattering volume seen by the detector results in the curve formed by the black circles. Finally, the effect of reflection correction with $R = 0.017 \pm 0.001$ is shown as open circles. The solid line is the result of a Mie calculation for an ensemble of spheres having a log-normal size distribution with $r_{\text{eff}} = 1.55$ μm, $v_{\text{eff}} = 0.0005$. The refractive index $n - in' = 1.191 - i0.005$, relative to HPLC water, at $\lambda = 633$ nm. The right panel shows corresponding $-F_{12}/F_{11}$ curves.

R of 0.017 ± 0.001, which was deduced by Schreurs (1996) by optimizing the comparison of the measurements on latex spheres with the results of Mie calculations. This value for R is about half of what is expected for normal incidence of the beam on both the cuvette and the basin. However, the beam is distorted by the cylindrical shape of the cuvette, which probably accounts for the lower value of R.

After applying the reflection correction on the latex sphere results, we found good agreement between measurements and results of Mie calculations, particularly for the F_{11} element. The discrepancies are largest at small and large scattering angles. Part of the differences between measurements and calculations may be due to the size distribution of the latex spheres not being perfectly log normal. Scanning electron microscope pictures of the latex spheres revealed that a few particles were larger than expected.

Error estimates—Total errors in the measurements result from several effects. In the first step of the data reduction procedure, the background contribution was subtracted. The two background functions were composed of an average of several F_{11}^{backgr} and F_{12}^{backgr} measurements (e.g., *see Fig. 5*). The statistical spread in these average background functions provided the first part of the error calculation. The length of the resulting error bars depends on the strength of the hydrosol scattering relative to the background scattering by the water. For some hydrosols, the background scattering at small and large angles was of similar magnitude to the scattering by the hydrosols themselves, which resulted in disproportionately large error bars, thereby rendering such data useless. For these cases, results are given for a smaller angle range than 20°–160°. In general, errors due to this background correction are largest at small and large angles.

Second, the effect of the uncertainty in the determination of the reflection coefficient $R = 0.017 \pm 0.001$ was calculated. The contribution to error bars of the individual measurements can become significant at large angles.

For samples in which the number of available measurements, N_{meas} (*see Table 1,* last column), was larger than one, weighted averages were calculated using the errors originating in the background correction and the reflection correction. The standard deviations combined with the errors mentioned above determined the total resulting error. For samples with only one measurement available, we used the error estimates of other measurements with approximately the same level of unprocessed signal, since we then expect the signal-to-noise level to be the same.

Results and discussion

Scattering functions, F_{11}, and $-F_{12}(\theta)/F_{11}(\theta)$ ratios were measured as functions of the scattering angle for 15 different samples of phytoplankton and 2 samples of silt (*see Table 1*). The results of these measurements are shown in Figs. 6–9. Figure 6 shows the results for species that are more or less spherically celled, Fig. 7 shows the results for filamentous phytoplankton, and Fig. 8 shows results for phytoplanktonic species that do not fit the above classifications. Finally, Fig. 9 depicts the results for Westerschelde silt. The measured values of F_{11} are scaled to the San Diego Harbor scattering function at 90°.

In Tables 2–5, the measured values of F_{11} are given that correspond to the data presented in Figs. 6–9, respectively. These tables are included to facilitate the use of these results, e.g., in the context of water-quality studies.

The errors of the measurement results indicated in Figs. 6–9 and Tables 2–5 reflect the combined effect of the main error sources (i.e., one standard deviation errors due to the statistical spread in the measurements themselves, one standard deviation errors due to the statistical spread in the background measurements, and one standard deviation errors due to the uncertainty in the determination of the reflection coefficient R). The magnitude of errors differs significantly from one species to another because of the difference in the maximum sample concentration that could be used. As a consequence, the scattering behavior of some species of phytoplankton is hard to measure accurately (e.g., Figs. 7b,d, 8d,e).

Scattering function behavior—In general, the shape of the measured scattering functions is similar to those reported for in situ measurements of seawater or other algal species (e.g., Kirk 1994 and references therein). The scattering functions, $F_{11}(\theta)$, are all strongly peaked in forward directions, but not equally so. For the angles covered, the flux ranges vary from 3 decades for *Phaeodactylum* (Fig. 8c) to only ~1 decade for *Microcystis* sp. and silt (Figs. 6c, 9b).

It is clear from Figs. 6–9 that the differences in scattering behavior are not easily derived from the morphology of the particles. For instance, the scattering behavior of the spherical *Microcystis* sp. (Fig. 6c) is similar to that of the cylindrical *Oscillatoria agardhii* (Fig. 7c). The occurrence of such similarities was also reported by Morel and Bricaud (1986), who found that their measured values of $F_{11}(\theta)$ of a cyanobacteria sample were similar to those of Privoznik et al. (1978) for a chlorophyta sample, *Chlorella pyrenoidosa.* Also, Sugihara et al. (1982) found a similar scattering behavior for two different suspensions of phytoplankton, *Chlorella* (more or less spherical cells) and *Ankistrodesmus falcatus* (long cylindrical cells).

In contrast, large differences in scattering behavior are found among the cylindrical phytoplankton (Fig. 7). Similar large differences are apparent between the three *Microcystis* samples (Fig. 6a,b,c). Note that the absence of gas vacuoles in one of the samples is the main difference between the samples corresponding to Fig. 6a and b.

Although most curves measured are smooth, in certain cases, structure is present. Pronounced oscillations over the total observed angle range are found for the filamentous species *Prochlorothrix hollandica* and *Melosira granulata* (Fig. 7a,d), which may result from the narrowness of the size distribution of the radii of the scattering cylinders, since resonances in the scattering pattern are more likely to occur for uniformly shaped particles with a narrow radius distribution (Stammes 1989). Filamentous species with cylindrical cells are more apt to have a narrow radius distribution than are single-celled species. This most probably accounts for the oscillations seen in the scattering functions of some of the filamentous phytoplankton (e.g., Fig. 7a,d).

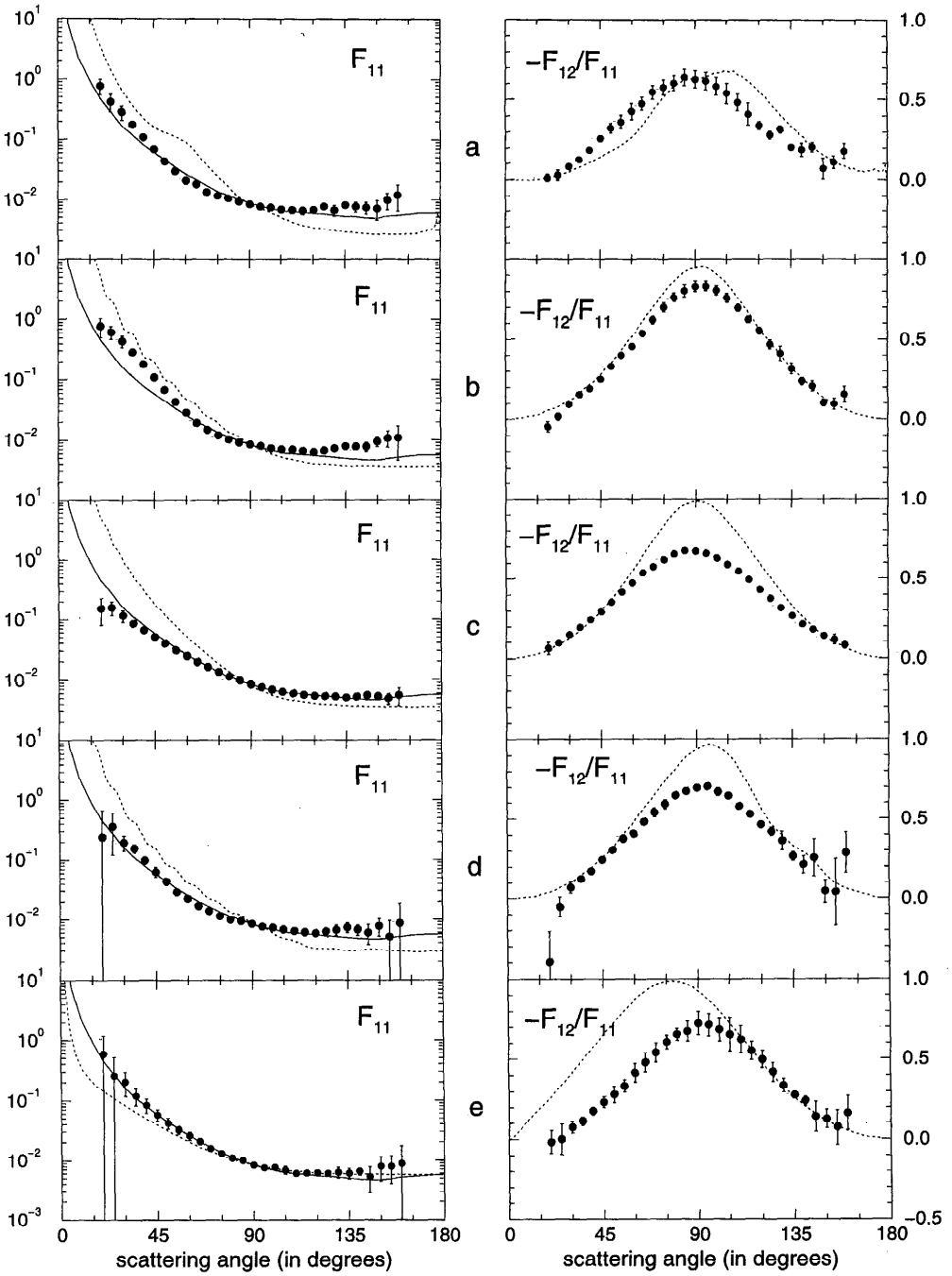

Fig. 6. The measured scattering functions, F_{11}, and ratios $-F_{12}/F_{11}$ are shown in the left and right panels, respectively (filled circles) for (a) *Microcystis aeruginosa* without gas vacuoles, (b) *Microcystis aeruginosa* with gas vacuoles, (c) *Microcystis* sp., (d) *Phaeocystis,* and (e) *Volvox aureus.* Also plotted are the scattering function for San Diego Harbor (solid, left panels) and the results of Mie calculations (dashed, left and right panels). The $F_{11}(\theta)$ functions are scaled at 90° to the scattering function of San Diego Harbor. Errors are smaller than symbols if no error bar is indicated.

For two of the phytoplankton species, *Microcystis aeruginosa* and *E. huxleyi,* the effect of a modification of the structural features was investigated. The scattering behavior of *M. aeruginosa* has been measured with and without gas vacuoles. In the latter case, the gas vacuoles were collapsed under pressure following the method of Dubelaar et al. (1987). At near-forward angles, the scattering function of *M. aeruginosa* with gas vacuoles (Fig. 6b) shows an unexpected decline toward smaller angles. This feature is absent for the same species without gas vacuoles (Fig. 6a). This suggests

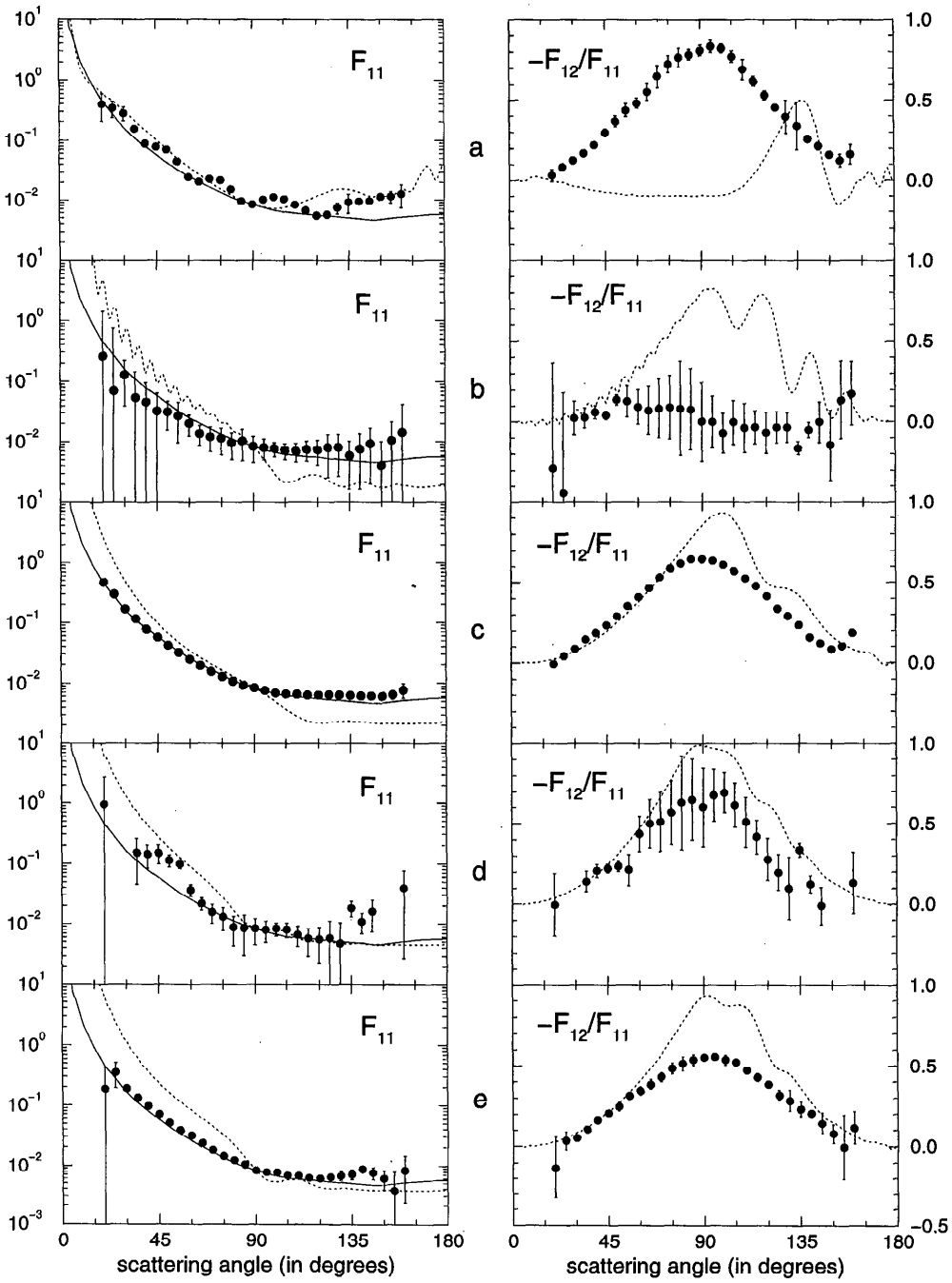

Fig. 7. Same as Fig. 6 for (a) *Prochlorothrix hollandica,* (b) *Oscillatoria amoena,* (c) *Oscillatoria agardhii,* (d) *Melosira granulata,* and (e) *Anabaena flos aquae.*

that gas vacuoles may be responsible for this feature. A similar, somewhat less pronounced feature occurs in the F_{11} curve of *Microcystis* sp. (Fig. 6c). Possibly, this feature may also be attributed in part to the presence of gas vacuoles.

The coccolithophorid *E. huxleyi* was studied with and without a calcite mantel. For the removal of the calcite mantel, carbon monoxide gas was used (Van Bleijswijk et al. 1994). Our measurements of both *E. huxleyi* with and without coccoliths are of poor quality (Fig. 8d,e). It is impossible to draw conclusions about the influence of the calcite mantels on the $F_{11}(\theta)$ behavior, except that both *E. huxleyi* samples scatter very little. This is consistent with the findings of Morel (1987) and Ackleson et al. (1994), for example, who argued that the reflectances observed for coccolithophore-dominated waters likely originated from the numerous detached coccoliths rather than from the living cells themselves.

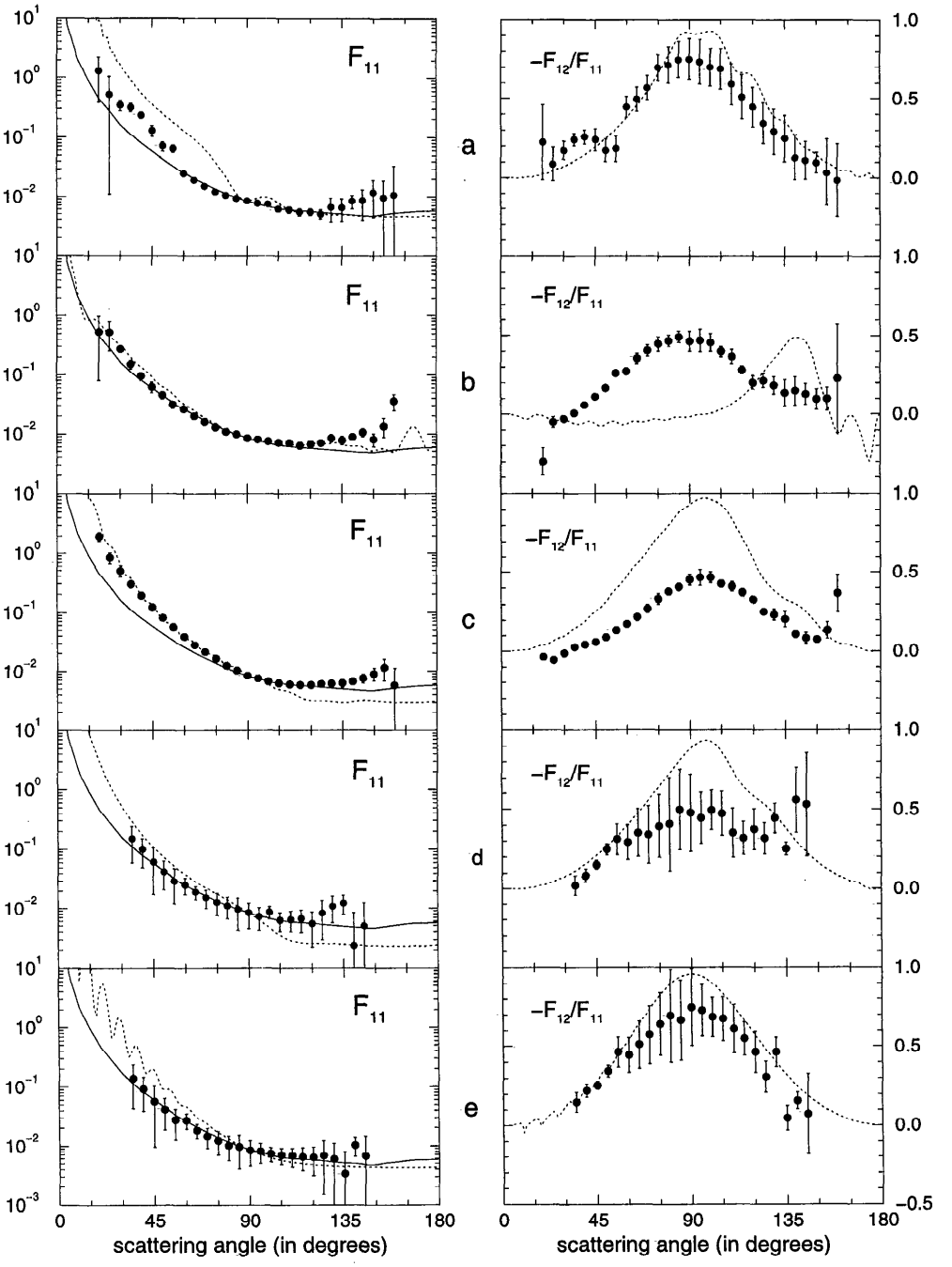

Fig. 8. Same as Fig. 6 for (a) *Astrionella formosa,* (b) *Selenastrum capricornutum,* (c) *Phaeodactylum,* (d) *Emiliania huxleyi* with coccoliths, and (e) *Emiliania huxleyi* without coccoliths.

The angular dependence of $-F_{12}(\theta)/F_{11}(\theta)$—Almost all measured $-F_{12}(\theta)/F_{11}(\theta)$ curves are similar in shape and show a maximum near a scattering angle of 90°. However, there are considerable differences in the height of the maxima, ranging from ~0.85 for *M. aeruginosa* with gas vacuoles and *Prochlorothrix* (Figs. 6b, 7a) to ~0.5 for *Selenastrum capricornutum* and *Phaeodactylum* (Fig. 8b,c) and even lower values (0.38 and 0.25) for silt (Fig. 9a and b, respectively). For *Oscillatoria amoena* (Fig. 7b), there is no maximum at all. However, the measurements of this species suffer from large errors.

The results are similar to what has been found for natural ocean water samples (Voss and Fry 1984; maxima between 0.6 and 0.8) and for phytoplankton samples grown in the laboratory (Fry and Voss 1985; Quinby-Hunt et al. 1989; maxima, ~0.8). Note that, in these cases, probably no corrections were made for the contribution of the water itself to the scattering.

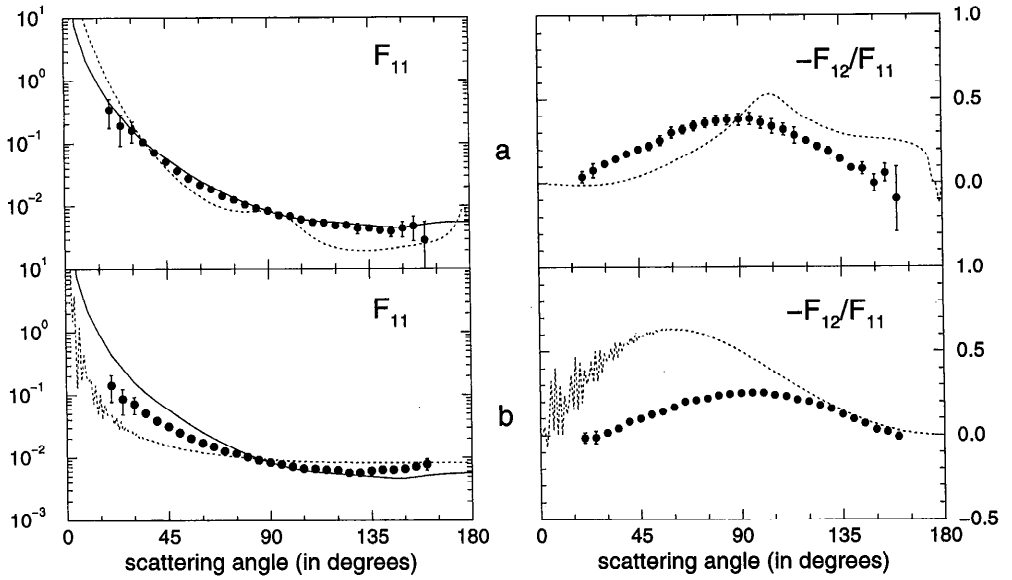

Fig. 9. Same as Fig. 6 for (a) Westerschelde silt with diameters ranging between 3 and 5 μm, and (b) Westerschelde silt with diameters ranging between 5 and 12 μm.

Table 2. Measured scattering functions F_{11} as functions of scattering angle for five phytoplankton species, corresponding to curves presented in Fig. 6. The digits in parentheses are the uncertainty in the last digits of the given value.

Scattering angle in degrees	*Microcystis aeruginosa* no gas vacuoles	*Microcystis aeruginosa* with gas vacuoles	*Microcystis* sp.	*Phaeocystis*	*Volvox aureus*
20.	0.76 (22)	0.76 (27)	0.153 (73)	0.24 (43)	0.59 (59)
25.	0.42 (13)	0.61 (15)	0.158 (41)	0.36 (24)	0.26 (25)
30.	0.282 (75)	0.430 (92)	0.115 (26)	0.195 (53)	0.205 (87)
35.	0.175 (14)	0.284 (13)	0.0857 (30)	0.158 (26)	0.121 (38)
40.	0.109 (10)	0.1804 (81)	0.0659 (18)	0.099 (14)	0.084 (23)
45.	0.0692 (71)	0.1090 (59)	0.0506 (15)	0.063 (12)	0.058 (12)
50.	0.0426 (49)	0.0682 (37)	0.03915 (86)	0.0439 (61)	0.0424 (88)
55.	0.0292 (28)	0.0424 (25)	0.03041 (78)	0.0286 (37)	0.0322 (47)
60.	0.0211 (28)	0.0283 (11)	0.02462 (16)	0.02257 (83)	0.0254 (39)
65.	0.0183 (12)	0.01928 (75)	0.01974 (07)	0.01718 (57)	0.0208 (23)
70.	0.0136 (13)	0.01476 (60)	0.01644 (17)	0.01395 (40)	0.0159 (16)
75.	0.0119 (11)	0.01206 (46)	0.01362 (17)	0.01159 (37)	0.01316 (88)
80.	0.01051 (82)	0.01011 (33)	0.01144 (07)	0.00994 (35)	0.01109 (59)
85.	0.00927 (88)	0.00910 (29)	0.00972 (04)	0.00941 (37)	0.00995 (62)
90.	0.00841 (80)	0.00841 (21)	0.00841 (03)	0.00841 (49)	0.00841 (44)
95.	0.00752 (82)	0.00781 (26)	0.00752 (05)	0.00756 (34)	0.00761 (31)
100.	0.00728 (84)	0.00719 (27)	0.00675 (08)	0.00718 (30)	0.00750 (32)
105.	000681 (88)	0.00698 (25)	0.00631 (07)	0.00671 (33)	0.0069 (10)
110.	0.00654 (84)	0.00684 (25)	0.00593 (08)	0.00641 (42)	0.00604 (53)
115.	0.00641 (85)	0.00657 (22)	0.00561 (11)	0.00612 (39)	0.00602 (43)
120.	0.00665 (60)	0.00628 (25)	0.00543 (12)	0.00584 (22)	0.00617 (51)
125.	0.00754 (54)	0.00664 (31)	0.00537 (13)	0.00630 (39)	0.00603 (66)
130.	0.0065 (14)	0.00729 (76)	0.00522 (26)	0.0066 (14)	0.0063 (13)
135.	0.00803 (77)	0.00782 (93)	0.00510 (22)	0.0074 (14)	0.0060 (12)
140.	0.0075 (14)	0.00775 (60)	0.00527 (21)	0.0067 (13)	0.00657 (91)
145.	0.0073 (17)	0.0077 (13)	0.00557 (38)	0.0060 (22)	0.0053 (24)
150.	0.0071 (26)	0.0095 (18)	0.00531 (50)	0.0077 (25)	0.0079 (35)
155.	0.0098 (31)	0.0108 (33)	0.00487 (95)	0.0050 (44)	0.0080 (38)
160.	0.0120 (57)	0.0109 (63)	0.0055 (18)	0.009 (10)	0.0087 (84)

Table 3. Measured scattering functions F_{11} as functions of scattering angle for five phytoplankton species, corresponding to curves presented in Fig. 7. The digits in parentheses are the uncertainty in the last digits of the given value.

Scattering angle in degrees	*Prochlorothrix hollandica*	*Oscillatoria amoena*	*Oscillatoria agardhii*	*Melosira granulata*	*Anabaena flos aquae*
20.	0.39 (19)	0.26 (1.17)	0.470 (69)	1.0 (1.8)	0.19 (24)
25.	0.34 (11)	0.07 (70)	0.298 (39)	—	0.35 (16)
30.	0.281 (72)	0.131 (91)	0.169 (24)	—	0.193 (24)
35.	0.157 (11)	0.055 (90)	0.1172 (28)	0.15 (11)	0.134 (18)
40.	0.0882 (55)	0.046 (51)	0.0789 (15)	0.143 (59)	0.098 (11)
45.	0.0780 (77)	0.033 (33)	0.0570 (14)	0.150 (52)	0.0711 (72)
50.	0.0711 (73)	0.032 (16)	0.04210 (67)	0.113 (25)	0.0512 (66)
55.	0.0450 (47)	0.027 (18)	0.03187 (43)	0.099 (16)	0.0385 (28)
60.	0.0249 (14)	0.0204 (79)	0.02472 (9)	0.0366 (79)	0.0315 (26)
65.	0.0205 (22)	0.0136 (49)	0.01940 (6)	0.0217 (49)	0.0233 (18)
70.	0.0231 (26)	0.0122 (54)	0.01542 (5)	0.0156 (54)	0.0181 (12)
75.	0.0219 (17)	0.0114 (54)	0.01283 (4)	0.0131 (54)	0.01452 (88)
80.	0.0152 (11)	0.0097 (45)	0.01089 (4)	0.0089 (45)	0.0125 (12)
85.	0.00942 (41)	0.0104 (55)	0.00930 (3)	0.0086 (55)	0.01063 (90)
90.	0.00841 (34)	0.0084 (39)	0.00841 (3)	0.0084 (39)	0.00841 (22)
95.	0.01004 (44)	0.0081 (30)	0.00754 (4)	0.0080 (30)	0.00785 (29)
100.	0.01121 (29)	0.0077 (20)	0.00698 (3)	0.0084 (20)	0.00776 (41)
105.	0.01030 (43)	0.0072 (22)	0.00664 (3)	0.0082 (22)	0.00687 (36)
110.	0.00828 (65)	0.0070 (24)	0.00657 (3)	0.0067 (24)	0.00682 (28)
115.	0.00661 (25)	0.0075 (27)	0.00634 (3)	0.0057 (27)	0.00627 (34)
120.	0.00548 (21)	0.0073 (32)	0.00631 (4)	0.0055 (32)	0.00611 (35)
125.	0.00561 (20)	0.0080 (53)	0.00643 (7)	0.0059 (53)	0.00642 (53)
130.	0.0072 (15)	0.0080 (53)	0.00637 (19)	0.0048 (56)	0.0068 (12)
135.	0.0092 (32)	0.0059 (43)	0.00629 (19)	0.0184 (52)	0.0072 (13)
140.	0.0094 (10)	0.0077 (60)	0.00609 (18)	0.0110 (40)	0.00875 (72)
145.	0.0097 (11)	0.0094 (73)	0.00616 (34)	0.0161 (87)	0.0077 (18)
150.	0.0112 (14)	0.0041 (60)	0.00602 (53)	—	0.0062 (23)
155.	0.0113 (25)	0.011 (11)	0.0065 (10)	—	0.0037 (42)
160.	0.0127 (54)	0.014 (28)	0.0077 (20)	0.040 (37)	0.0084 (61)

We found the highest maxima of $-F_{12}/F_{11}$ for phytoplankton species that contain gas vacuoles. Gas vacuoles strongly influence the behavior of $-F_{12}/F_{11}$. This follows most clearly from the curves of *M. aeruginosa* with and without gas vacuoles (Fig. 6a,b). In this case, the gas vacuoles cause an increase of $-F_{12}/F_{11}$ from ~0.65 to 0.85 at 90°. Indeed, on theoretical grounds, we expect $-F_{12}/F_{11}$ to be higher for smaller particles, such as gas vacuoles (Van de Hulst 1957, chap. 6; Bohren and Huffman 1983, chaps. 5, 13). In contrast, $-F_{12}/F_{11}$ is expected to decrease for higher refractive indices. This agrees with what we observe for the curves of *E. huxleyi* with and without coccoliths (Fig. 8d,e). After removal of the calcium carbonate coccoliths (n = 1.2), the maximum in the $-F_{12}/F_{11}$ curve increases from ~0.5 to 0.75. The expected decrease for higher refractive indices is also in agreement with the fact that we find the lowest significant values of $-F_{12}/F_{11}$ for the inorganic silt particles. Therefore, investigations of $-F_{12}/F_{11}$ values near 90° may provide a useful tool to distinguish between organic and inorganic scattering material.

For $-F_{12}/F_{11}$ curves, an enhancement at backscattering angles is observed for *M. aeruginosa, Phaeocystis, Oscillatoria agardhii,* and *Phaeodactylum* (Figs. 6a,b,d, 7c, 8c). However, these enhancements are usually accompanied by large error bars, because in this region, the errors (because of inaccuracies in background and reflection correction) can be large.

Comparison of scattering measurements with Mie calculations—Because Mie theory holds only for spherical homogeneous particles, phytoplankton and silt particles usually have internal or external structures too complex to justify using Mie calculations to model their scattering behaviors. However, compared to other light-scattering computations, Mie calculations can be performed relatively quickly. They require relatively few input parameters that, in principle, can be readily measured or estimated, namely, the size distribution and the complex refractive index. Therefore, we investigated whether results of Mie calculations produce reasonable approximations of the measured results, particularly when using measured or estimated input parameters.

The dashed lines in Figs. 6–9 represent results of Mie calculations, both for the scattering functions (left panels), also scaled to the San Diego Harbor scattering function at 90°, and the angular distributions of $-F_{12}/F_{11}$ (right panels). The parameters used for these calculations, i.e., size distributions of volume-equivalent spheres and real and complex parts of the refractive indices, are given in Table 1. For the Mie calculations, we used measured input parameters or, if not available, values from Bricaud and Morel (1986) (*see*

Table 4. Measured scattering functions F_{11} as functions of scattering angle for five phytoplankton species, corresponding to curves presented in Fig. 8. The digits in parentheses are the uncertainty in the last digits of the given value.

Scattering angle in degrees	*Astrionella formosa*	*Selenastrum capricornutum*	*Phaeodactylum*	*Emiliania huxleyi* with coccoliths	*Emiliania huxleyi* no coccoliths
20.	1.30 (92)	0.53 (45)	1.96 (32)	—	—
25.	0.52 (51)	0.52 (27)	0.84 (17)	—	—
30.	0.356 (72)	0.274 (35)	0.50 (11)	—	—
35.	0.317 (53)	0.151 (26)	0.296 (13)	0.151 (29)	0.138 (96)
40.	0.233 (30)	0.095 (14)	0.1922 (78)	0.101 (51)	0.092 (53)
45.	0.130 (26)	0.063 (13)	0.1222 (89)	0.062 (45)	0.056 (47)
50.	0.072 (13)	0.0453 (62)	0.0812 (39)	0.043 (22)	0.041 (23)
55.	0.0648 (82)	0.0310 (40)	0.0563 (41)	0.030 (18)	0.027 (15)
60.	0.0249 (16)	0.02628 (80)	0.0388 (18)	0.0253 (79)	0.0268 (79)
65.	0.0191 (10)	0.01996 (49)	0.0278 (17)	0.0191 (49)	0.0181 (49)
70.	0.01513 (86)	0.01585 (45)	0.0213 (12)	0.0154 (54)	0.0145 (54)
75.	0.01207 (82)	0.01301 (39)	0.01626 (78)	0.0128 (54)	0.0123 (54)
80.	0.01052 (77)	0.01088 (38)	0.01251 (72)	0.0112 (45)	0.0101 (45)
85.	0.00929 (70)	0.00980 (35)	0.01022 (56)	0.0097 (55)	0.0096 (55)
90.	0.00841 (70)	0.00841 (36)	0.00841 (54)	0.0084 (39)	0.0084 (39)
95.	0.00769 (71)	0.00803 (35)	0.00756 (71)	0.0073 (30)	0.0080 (30)
100.	0.00736 (70)	0.00748 (35)	0.00667 (40)	0.0087 (20)	0.0074 (20)
105.	0.00611 (71)	0.00709 (36)	0.00630 (32)	0.0063 (22)	0.0070 (22)
110.	0.00588 (72)	0.00695 (36)	0.00593 (46)	0.0064 (24)	0.0068 (24)
115.	0.00540 (71)	0.00632 (34)	0.00579 (51)	0.0066 (27)	0.0065 (27)
120.	0.00544 (72)	0.00659 (37)	0.00579 (16)	0.0055 (32)	0.0064 (32)
125.	0.00501 (91)	0.00694 (45)	0.00599 (22)	0.0083 (53)	0.0068 (53)
130.	0.0066 (28)	0.0085 (14)	0.00612 (81)	0.0110 (53)	0.0060 (50)
135.	0.0065 (27)	0.0078 (13)	0.00623 (98)	0.0123 (45)	0.0034 (46)
140.	0.0083 (22)	0.0089 (11)	0.00670 (90)	0.0024 (60)	0.0102 (36)
145.	0.0086 (46)	0.0106 (17)	0.0076 (13)	0.0051 (74)	0.0067 (79)
150.	0.0117 (74)	0.0080 (20)	0.0090 (22)	—	—
155.	0.0097 (91)	0.0135 (47)	0.0114 (46)	—	—
160.	0.011 (23)	0.036 (11)	0.0057 (91)	—	—

Table 1). Unfortunately, not all parameters for r_{eff}, v_{eff}, and n' could be established. In such cases, we present results of Mie calculations with parameters that yield the best fit to the measured data.

In general, results of Mie calculations differ significantly from the measured data, both for F_{11} and $-F_{12}/F_{11}$. Similar results have been reported by others (e.g., Sugihara et al. 1983; Quinby-Hunt et al. 1989). Most often, the Mie calculations produce a steeper scattering function, F_{11}, than the measured function and the San Diego Harbor scattering function. Note that when a Mie function is not too steep, the measured or fitted complex refractive index has a real and/or imaginary part that is larger than expected, at least for the bulk complex refractive index (i.e., $n > 1.08$ and/or $n' > 0.02$).

The difficulties in reproducing the measurement results using Mie theory become especially clear from the fitted v_{eff} and n' parameters that often attain extreme values. For example, for the smaller silt particles, the fitted v_{eff} is extremely broad, since $v_{eff} = 0.5$ is the maximum value possible for a gamma distribution. In contrast, the fitted v_{eff} of the larger particles is zero, causing strong oscillations in the the resulting Mie curves, which are not observed in the measurements. Likewise, for the two silt samples, the fitted values of n' go to opposite extremes.

In summary, results of Mie calculations using a priori known or estimated input parameters do not generally produce good approximations to the scattering behavior of phytoplankton and silt, although, in some cases, the results of measurements and calculations seem to agree reasonably well.

Comparison with the San Diego Harbor scattering function—A comparison of measurements of the element F_{11} with a scattering function of San Diego Harbor water (solid lines, Petzold 1972) is also shown in Figs. 6–9. This function was measured at a wavelength of 514 nm with a 75-nm bandwidth. It is frequently used in modeling remotely sensed reflectance of turbid waters (e.g., Dekker 1993; Kirk 1994), which is the reason we chose this function as a standard to compare our results with, even though Petzold's (1972) results pertain to in situ measurements of natural waters rather than to laboratory measurements of individual phytoplankton species like ours. The measured scattering functions have been scaled to the San Diego Harbor scattering function at 90°.

The San Diego function is strongly peaked in the forward direction and rather flat at backward angles. In contrast, most of the measured scattering functions show an increase at backward angles, with the possible exceptions of *Microcystis*

Table 5. Measured scattering functions F_{11} as functions of scattering angle for two Westerschelde silt samples, corresponding to the curves in Fig. 9, plus the San Diego Harbor scattering function (Petzold 1972). The digits in parentheses are the uncertainty in the last digits of the given value.

Scattering angle in degrees	Westerschele silt 3–5 μm	Westerschelde silt 5–12 μm	San Diego Harbor Petzold (1972)
20.	0.34 (17)	0.143 (66)	0.4452
25.	0.189 (98)	0.087 (38)	0.2734
30.	0.160 (57)	0.071 (22)	0.1613
35.	0.1067 (65)	0.0510 (26)	0.1109
40.	0.0728 (37)	0.0384 (15)	0.07913
45.	0.0510 (32)	0.0317 (13)	0.05858
50.	0.0366 (21)	0.02501 (83)	0.04388
55.	0.0278 (17)	0.02046 (68)	0.03288
60.	0.02181 (81)	0.01737 (32)	0.02548
65.	0.01838 (62)	0.01498 (24)	0.02041
70.	0.01441 (70)	0.01264 (28)	0.01655
75.	0.01243 (56)	0.01155 (22)	0.01345
80.	0.01064 (36)	0.01033 (14)	0.01124
85.	0.00941 (49)	0.00911 (20)	0.00964
90.	0.00841 (42)	0.00841 (17)	0.00841
95.	0.00723 (45)	0.00779 (18)	0.00740
100.	0.00697 (38)	0.00718 (16)	0.00669
105.	0.00618 (44)	0.00666 (18)	0.00622
110.	0.00558 (34)	0.00663 (15)	0.00589
115.	0.00549 (42)	0.00631 (18)	0.00573
120.	0.00498 (22)	0.00622 (11)	0.00555
125.	0.00507 (16)	0.00577 (9)	0.00534
130.	0.00446 (82)	0.00573 (36)	0.00515
135.	0.00445 (40)	0.00610 (21)	0.00497
140.	0.00418 (51)	0.00630 (30)	0.00482
145.	0.00402 (74)	0.00634 (41)	0.00464
150.	0.0045 (12)	0.00656 (63)	0.00463
155.	0.0049 (21)	0.00713 (77)	0.00490
160.	0.0029 (46)	0.0078 (16)	0.00514

sp., *O. agardhii,* and the small silt particles (Figs. 6c, 7c, 9a).

To get a better impression of the overall differences in shape between the measured scattering functions and the San Diego Harbor scattering function, we plotted (Fig. 10a) a subset of four measured scattering functions divided by the San Diego Harbor scattering function (Petzold 1972). This subset is representative of the differences in shape among the whole set of phytoplankton functions and has been selected for having relatively high signal-to-noise ratios. Again, the scattering functions have been normalized at 90°. In Fig. 10b, the same is shown for the two silt samples.

It is clear from Fig. 10a that the differences in the shapes of the scattering functions of the phytoplankton can be large. In forward directions, the differences in steepness between the scaled functions are up to about a factor of 10, although a factor of 2 is more common. In this range, functions are found both below and above the San Diego Harbor standard. Remarkably, in backward regions, the discrepancies in shape relative to the standard can also be large, up to about a factor of 6 for the scaled functions, but beyond 90°, all scattering functions of phytoplankton are found above (or equal to) the standard of San Diego Harbor water.

In Fig. 10b, the scattering function of the smaller silt particles resembles the San Diego standard rather well (*see Fig. 9a*). This is probably not a coincidence, since silt is an important particle constituent in Harbor water (Petzold 1972). However, the scattering function of the larger silt particles differs considerably from the San Diego Harbor function. This function, normalized to the standard function, is about a factor of 7 lower in the forward direction, thus indicating that particle size is an important parameter for the light-scattering behavior of these irregular particles.

Conclusion

The measured scattering functions $F_{11}(\theta)$ presented here are used in the context of water-quality studies (Dekker et al. 1996). Shapes of the scattering functions of phytoplankton show substantial differences, even though the results of these measurements show some features (e.g., scattering functions $F_{11}(\theta)$ being peaked in forward directions, as well as more or less bell-shaped $-F_{12}(\theta)/F_{11}(\theta)$ functions) similar to those reported for in situ measurements of seawater and other algal species (e.g., Kirk 1994 and references therein).

In forward directions, the differences between the scattering functions scaled at 90° are up to about a factor of 10 (although a factor of 2 is more common) both below and above the San Diego Harbor standard. In backward regions, the differences between the scaled scattering functions are also large, up to about a factor of 6. All scattering functions of phytoplankton beyond 90° are found above (or equal to) the standard of San Diego Harbor water. Only 3 of the 17 measured scattering functions resemble the San Diego Harbor scattering function closely, most notably in the case of smaller silt particles.

Large differences in shapes of the scattering functions may yield a considerable bias in water-quality algorithms that are based on the San Diego standard. If one uses an empirical approach to remote sensing of water quality, large scatter in the data may be expected unless waterbodies are first classified according to the dominant scattering particles followed by establishment of empirical relationships for each water type.

The scattering behavior is not easily predicted from the morphology of the particles. Spherically and cylindrically celled species may, for instance, produce similar results, whereas two spherical species may yield quite different results. Overall, cylindrically celled species seem to have a higher probability of oscillations in the scattering function, probably due to a narrower size distribution of the radii of cylindrically shaped cells compared to cells with other shapes.

Structural features, such as gas vacuoles, inside phytoplankton play an important role in the scattering behavior of phytoplankton (e.g., Dubelaar et al. 1987; Ganf et al. 1989). Gas vacuoles may be responsible for a remarkable feature in the F_{11} curves of some of the phytoplankton samples (i.e., an unexpected decline toward smaller angles). This feature is observed clearly for *M. aeruginosa* with gas vacuoles, but

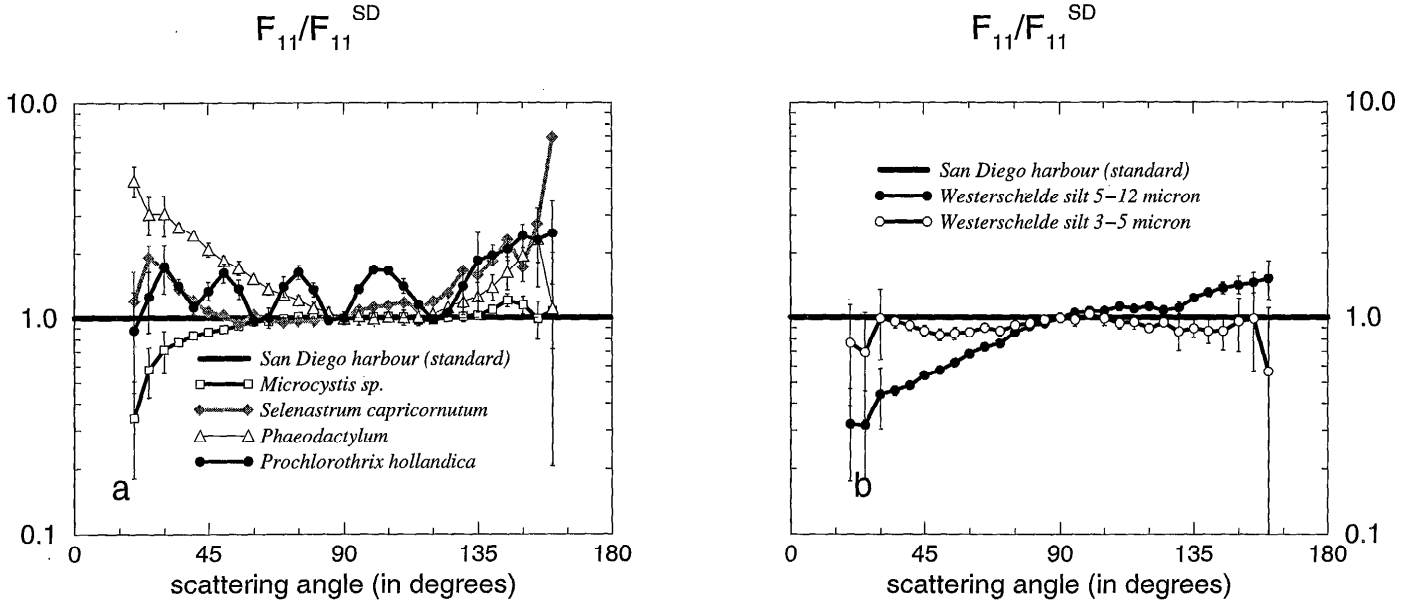

Fig. 10. Measured scattering functions divided by the San Diego Harbor scattering function (Petzold 1972) scaled at 90°, F_{11}/F_{11}^{SD}, are plotted for (a) *Microcystis* sp., *Phaeodactylum, Prochlorothrix hollandica,* and *Selenastrum capricornutum;* (b) Westerschelde silt with diameters ranging between 3 and 5 μm, and Westerschelde silt with diameters ranging between 5 and 12 μm.

it is completely absent for the same species without gas vacuoles. In addition, gas vacuoles cause a significant increase of $-F_{12}/F_{11}$ at side-scattering angles. This again follows most clearly from a comparison between the curves of *M. aeruginosa* with and without gas vacuoles. The presence of coccoliths in *E. huxleyi,* by contrast, causes a significant decrease in the $-F_{12}/F_{11}$ curve around 90°.

For the measured $-F_{12}/F_{11}$ curves, we find considerable differences in the height of the maxima at ~90°, ranging from ~0.85 for *Prochlorothrix* and *M. aeruginosa* with gas vacuoles to values of ~0.25 for silt, suggesting that it may be possible to distinguish between phytoplankton and mineral scatterers by using the maximal height of the $-F_{12}/F_{11}$ function as a criterion.

In general, we have found no good agreement between results of our measurements and results of Mie calculations. Apart from effects of nonsphericity, another reason our Mie calculations, using overall sizes and bulk refractive indices, did not agree well with the measurements of F_{11} and $-F_{12}/F_{11}$ could relate to structural features of the cell. An increase in the refractive index, for example, or a decrease in the size of the particles produces a less peaked Mie scattering function (*see* Bohren and Huffman 1983; Morel and Bricaud 1986). Therefore, it is interesting to investigate whether input parameters different from those used for our Mie calculations might yield a better description of the measured scattering patterns (Schreurs 1996). It is probable that more sophisticated scattering approaches are required to describe the scattering behavior of phytoplankton and silt. For instance, calculations for coated spheres (Meyer 1979) indicate that their scattering functions are less peaked in the forward direction than those of uncoated spheres. Scattering matrix elements computed for coated spheres compared well with the corresponding elements measured for (spherical) *Chlorella* particles (Quinby-Hunt et al. 1989).

The scattering behavior of some filamentous species (e.g., *Prochlorothrix hollandica* and *Melosira granulata,* Fig. 8a,d) may approximate those of infinitely long cylinders, for which computer codes are available (Stammes 1989). We are presently comparing measured scattering patterns of these phytoplankton species with those calculated for infinitely long cylinders (Schagen 1997). Alternatives may be offered by calculations for (coated) ellipsoids (Cross and Latimer 1972; Farafonov et al. 1996), discrete-dipole approximation calculations (Lumme and Rahola 1994), and T-matrix calculations (Mishchenko et al. 1996).

Clearly, the scattering properties of natural water constituents are diverse and interesting enough not only to call for more detailed scattering calculations, but also for more elaborate measurements. In particular, there is a need for more measurements on clay particles as well as detritus from algae and peat, since these are frequently important constituents of natural waters. Furthermore, measurements over a wider range of scattering angles than attained in our study are desirable.

References

AAS, E. 1981. The refractive index of phytoplankton. Inst. Rep. Ser., Univ. Oslo **46:** 61.

ACKLESON, S. G., W. M. BALCH, AND P. M. HOLLIGAN. 1994. Response of water-leaving radiance to particulate calcite and chlorophyll *a* concentrations: A model for Gulf of Maine coccolithophore blooms. J. Geophys. Res. **99:** 7483–7499.

———, J. J. CULLEN, J. BROWN, AND M. LESSER. 1993. Irradiance-induced variability in light scatter from marine phytoplankton in culture. J. Plankton Res. **15:** 737–760.

———, AND R. W. SPINRAD. 1988. Size and refractive index of individual marine particulates: A flow cytometric approach. Appl. Opt. **27:** 1270–1277.

BOHREN, C. F., AND D. R. HUFFMAN. 1983. Absorption and scattering of light by small particles. Wiley.

BRICAUD, A., AND A. MOREL. 1986. Light attenuation and scattering by phytoplanktonic cells: A theoretical modelling. Appl. Opt. **25:** 571–580.

CARDER, K. L., R. D. TOMLINSON, AND G. F. BEARDSLEY. 1972. A technique for the estimation of indices of refraction of marine phytoplankters. Limnol. Oceanogr. **17:** 833–839.

CROSS, D. A., AND P. LATIMER. 1972. Angular dependence of scattering from *Escherichia coli* cells. Appl. Opt. **11:** 1225–1228.

DEKKER, A. G. 1993. Detection of optical water quality parameters for eutrophic waters by high resolution remote sensing. Ph.D. thesis, Free Univ., Amsterdam.

———, H. J. HOOGENBOOM, H. VOLTEN, R. SCHREURS, AND J. F. DE HAAN. 1996. Angular scattering functions of algae and silt: An analysis of backscattering to scattering fraction. SPIE Conference Ocean Optics XIII, 22–25 October, Halifax, Canada.

———, T. J. MALTHUS, AND H. J. HOOGENBOOM. 1995. The remote sensing of inland water quality, p. 123–142. *In* F. M. Danso and S. E. Plummer [eds.], Advances in environmental remote sensing. Wiley.

DONZE, M., G. B. J. DUBELAAR, AND J. W. M. VISSER. 1987. Anomalous behaviour of forward and perpendicular light scattering of a cyanobacterium due to intracellular gas vacuoles. BCRS Report 87–08.

DUBELAAR, G. B. J., J. W. M. VISSER, AND M. DONZE. 1987. Anomalous behaviour of forward and perpendicular light scattering of a cyanobacterium due to intracellular gas vacuoles. Cytometry **8:** 405–412.

FARAFONOV, V. G., N. V. VOSHCHINNIKOV, AND V. V. SOMSIKOV. 1996. Light scattering by a core-mantle spheroidal particle. Appl. Opt. **35:** 5412–5426.

FRY, E. S., AND K. J. VOSS. 1985. Measurements of the Mueller matrix for phytoplankton. Limnol. Oceanogr. **30:** 1322–1326.

GANF, G. G., R. L. OLIVER, AND A. E. WALSBY. 1989. Optical properties of gasvacuolate cells and colonies of *Microcystis* in relation to light attenuation in a turbid stratified reservoir (Mount Bold Reservoir, South Australia). Aust. J. Mar. Freshwater Res. **40:** 595–611.

HANSEN, J. E., AND L. D. TRAVIS. 1974. Light scattering in planetary atmospheres. Space Sci. Rev. **16:** 527–610.

HOVENIER, J. W. [ED.]. 1996. Light scattering by non-spherical particles. J. Quant. Spectrosc. Radiat. Transfer (special issue) **55:** 535–694.

———, H. C. VAN DE HULST, AND C. VAN DE MEE. 1986. Conditions for the elements of the scattering matrix. Astron. Astrophys. **157:** 301.

HUNT, A. J., AND D. R. HUFFMAN. 1973. A new polarization-modulation light scattering instrument. Rev. Sci. Instrum. **44:** 1753–1762.

KIRK, J. T. O. 1994. Light and photosynthesis in aquatic ecosystems. CSIRO, Canberra, Australia. Cambridge Univ. Press.

KRÓL, T., A. ZIELINSKI, AND K. WITKOWSKI. 1992. Light scattering on *Chlorella vulgaris* cell. SPIE Vol. 1750, Ocean Optics XI, 47–54.

KUIK, F. 1992. Single scattering of light by ensembles of particles with various shapes. Ph.D. thesis, Free Univ., Amsterdam.

———, P. STAMMES, AND J. W. HOVENIER. 1991. Experimental determination of scattering matrices of water droplets and quartz particles. Appl. Opt. **30:** 4872–4881.

KULLENBERG, G. 1984. Observations of light scattering functions in two oceanic areas. Deep-Sea Res. **31:** 295–316.

LOFFTUS, K. D., M. S. QUINBY-HUNT, A. J. HUNT, F. LIVOLANT, AND M. MAESTRE. 1992. Light scattering by *Prorocentrum micans*: A new method and results. Appl. Opt. **31:** 2924–2931.

LUMME, K., AND J. RAHOLA. 1994. Light scattering by porous dust particles in the discrete-dipole approximation. Astrophys. J. **425:** 653–667.

MEYER, R. A. 1979. Light scattering from biological cells: Dependence of backscatter radiation on membrane thickness and refractive index. Appl. Opt. **18:** 585–588.

MIE, G. 1908. Beiträge zur Optik trüber Medien speziell kolloidaler Metallösungen. Ann. Phys. **25:** 377.

MISHCHENKO, M. I., L. D. TRAVIS, AND D. W. MACKOWSKI. 1996. T-matrix computations of light scattering by nonspherical particles: A review. J. Quant. Spectrosc. Radiat. Transfer **55:** 535–575.

MOBLEY, C. D. 1994. Light and water, radiative transfer in natural waters. Academic.

MOREL, A. 1987. Chlorophyll-specific scattering coefficient of phytoplankton. A simplified theoretical approach. Deep-Sea Res. **34:** 1093–1105.

———, AND A. BRICAUD. 1986. Inherent optical properties of algal cells including picoplankton: Theoretical and experimental results. Can. Bull. Aquat. Sci. **214:** 521–559.

PETZOLD, T. L. 1972. Volume scattering functions for selected ocean waters. Scripps Inst. Oceanogr. Visibility Lab., Ref. 72–78.

PRIVOZNIK, K. G., K. J. DANIEL, AND F. P. INCROPERA. 1978. Absorption, extinction, and phase function measurements for algal suspensions of *Chlorella pyrenoidosa*. J. Quant. Spectrosc. Radiat. Transfer **20:** 345–352.

QUINBY-HUNT, M. S., A. J. HUNT, K. D. LOFFTUS, AND D. SHAPIRO. 1989. Polarized-light scattering studies of marine *Chlorella*. Limnol. Oceanogr. **34:** 1587–1600.

SCHAGEN, M. 1997. Numerical calculation of the scattering properties of cylindrical phytoplankton. Graduation Report, Free Univ., Amsterdam.

SCHNABLEGGER, H., AND O. GLATTER. 1993. Simultaneous determination of size distribution and refractive index of colloidal particles from static light-scattering experiments. J. Colloid Interface Sci. **158:** 228–242.

SCHREURS, R. 1996. Light scattering by algae: Fitting experimental data using Lorenz-Mie theory. Graduation Report, Free Univ., Amsterdam.

SHELDON, R. W., AND T. R. PARSONS. 1967. A practical manual on the use of the Coulter counter in marine science. Coulter Electronics.

SPILHAUS, A. F. 1968. Observations of light scattering in seawater. Limnol. Oceanogr. **13:** 418–422.

SPINRAD, R. W., AND J. F. BROWN. 1986. Relative real refractive index of marine microorganisms: A technique for flow cytometric estimation. Appl. Opt. **25:** 1930.

STAMMES, P. 1989. Light scattering properties of aerosols and the radiation inside a planetary atmosphere. Ph.D. thesis, Free Univ., Amsterdam.

STRAMSKI, D., AND A. MOREL. 1990. Optical properties of photosynthetic picoplankton in different physiological states as affected by growth irradiance. Deep-Sea Res. **37:** 245–266.

SUGIHARA, S., M. KISHINO, AND N. OKAMI. 1982. Back-scattering of light by particles suspended in water. Phys. Chem. Res. **76:** 1–8.

VAN BLEIJSWIJK, J. D. L., R. S. KEMPERS, M. J. VELDHUIS, AND P. WESTBROEK. 1994. Cell and growth characteristics of types A and B of *Emiliania huxleyi* (prymnesiophycae) as determined by flow cytometry and chemical analysis. J. Phycol. **30:** 230–241.

VAN DE HULST, H. C. 1957. Light scattering by small particles. Wiley.

VOSS, K. J., AND E. S. FRY. 1984. Measurement of the Mueller matrix for ocean water. Appl. Opt. **23:** 4427–4439.

WALSBY, A. E. 1994. Gas vesicles. Microbiol. Rev. **58:** 94–144.

WHITLOCK, C. H., L. R. POOLE, J. W. USRY, W. M. HOUGHTON, W. G. WITTE, W. D. MORRIS, AND E. A. GURGANUS. 1981. Comparison of reflectance with backscatter and absorption parameters for turbid waters. Appl. Opt. **20:** 517–522.

WITKOWSKI, K., L. WOLINSKI, Z. TURZYNSKI, D. GEDZIOROWSKA, AND A. ZIELINSKI. 1993. The investigation of kinetic growth of *Chlorella vulgaris* cells by the method of integral and dynamic light scattering. Limnol. Oceanogr. **38:** 1365–1372.

Received: 10 April 1997
Accepted: 6 January 1998
Amended: 2 June 1998